Donor−Acceptor-Assisted Diels−Alder Reaction of Anthracene and Tetracyanoethylene

Kristopher E. Wise and Ralph A. Wheeler*

Department of Chemistry & Biochemistry, 620 Parrington Oval, Room 208, University of Oklahoma, Norman, Oklahoma 73019

Received: March 24, 1999; In Final Form: August 10, 1999

We report hybrid Hartree−Fock/density functional B3LYP/6-31G(d) and B3LYP/6-31+G(d,p) calculations to determine the path of the Diels−Alder reaction between anthracene and tetracyanoethylene (TCNE) and to characterize the stationary points along the path. With only one exception, calculated bond distances in anthracene, TCNE, and $TCNE^{\bullet-}$ (the limiting case of complete electron donation to TCNE) are within 3 standard deviations of experiment. We also predict the geometry of $anthracene^{\bullet+}$. Calculations to determine the reaction path establish unambiguously that the observed electron donor−acceptor complex is an intermediate and that donor−acceptor interactions assist attainment of the reaction's transition state by lowering the energy barrier to pyramidalizing about C_9/C_{10} of anthracene and the ethylenic carbons of TCNE. Combined with thermodynamic integration calculations in chloroform solvent, B3LYP calculations of the activation energy (20.1 kcal/mol) agree quantitatively with the experimentally derived activation energy (20.0 kcal/mol). For the retro-Diels−Alder reaction, the calculated activation energy underestimates the experimental value by 4.6−5.0 kcal/mol, suggesting that B3LYP/6-31G(d) and B3LYP/6-31+G(d,p) calculations understabilize the reaction product.

Introduction

The Diels−Alder reaction of anthracene and tetracyanoethylene (TCNE), depicted in Figure 1, is the central figure in a mystery that is unresolved after more than four decades of study. The transient blue-green color observed upon mixing anthracene and TCNE (reminiscent of the color change seen in the very first Diels−Alder reaction[1]) and the corresponding broad absorption bands in the UV−vis spectra are telltale signs of electron donor−acceptor (EDA) complex formation in the reaction mixture.[2−7] The major, unresolved debate surrounding this and closely related reactions is whether the Diels−Alder reaction proceeds through the EDA complex intermediate (right side of Figure 1) or directly from the reactants to the adduct, with the EDA complex formation as a nonproductive side equilibrium (left side of Figure 1).[8−12] Two possible steady-state rate constant expressions, both consistent with published kinetic studies, may be written for the reactions on the right and left sides of Figure 1, respectively:

$$k_{exp} = k_1 K_{DA}/(1 + K_{DA}[TCNE]) \quad (1)$$

$$k_{exp} = k_2/(1 + K_{DA}[TCNE]) \quad (2)$$

Due to the kinetic indistinguishability of eqs 1 and 2, neither proposed mechanism can be eliminated. So the question of whether the EDA complex is formed as a nonproductive side equilibrium of the cycloaddition reaction or is actually an intermediate on the reaction path between the isolated reactants and the transition state has yet to be answered conclusively.[10−12]

Despite these difficulties, experimental work strongly suggests the intermediacy of the EDA complex in the closely related reaction of 9,10-dimethylanthracene and TCNE.[9] These experiments imply that if the reaction proceeds through the EDA complex, then the observed negative activation enthalpy ($\Delta H^{\ddagger}_{exp}$) will be a sum of the enthalpy of EDA complex formation

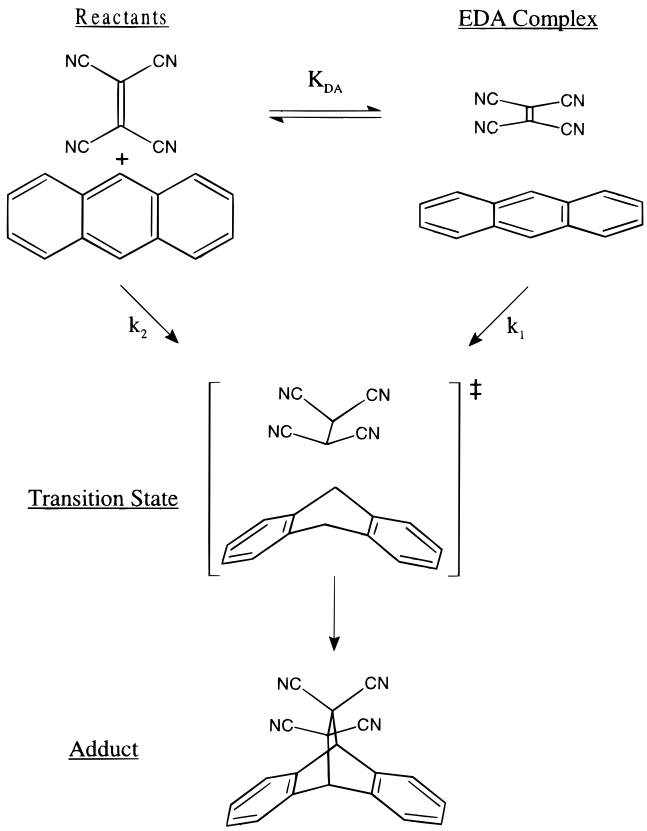

Figure 1. Schematic representation of two possible reaction mechanisms for the Diels−Alder cycloaddition of anthracene and tetracyanoethylene.

10.1021/jp991012d CCC: $18.00
Published on Web 09/23/1999

($\Delta H°_{DA}$) and the activation enthalpy for conversion of the complex to the transition state ($\Delta H^{‡}_1$):

$$\Delta H^{‡}_{exp} = \Delta H°_{DA} + \Delta H^{‡}_1$$

If, on the other hand, the EDA complex is involved in an unproductive equilibrium, the observed activation enthalpy is simply the enthalpy of activation from separated reactants to the transition state. Reasoning that the activation enthalpy $\Delta H^{‡}_1$ must be positive, the authors concluded that $\Delta H°_{DA}$ must make a substantial negative contribution to the observed activation energy. Unfortunately, the experimental separation of $\Delta H^{‡}_{exp}$ into its components ($\Delta H°_{DA}$ and $\Delta H^{‡}_1$) has not yet been accomplished. Moreover, the assumption that the activation enthalpy $\Delta H^{‡}_1$ must be positive has been questioned by workers studying other cycloaddition reactions that exhibit negative activation enthalpies in the absence of EDA complex formation.[13]

While an experimental resolution to the EDA complex's role in this reaction remains elusive, the size of the system has thus far prevented its study by high-level quantum chemical methods. Continuing development of both powerful computing resources and accurate and efficient computational methods, specifically density functional methods,[14−16] now make this work possible. In this paper we summarize the structures and relative energetics of all stationary points along the reaction coordinate and show them to be connected by using an intrinsic reaction coordinate mapping procedure.[17−19] Each stationary point has been optimized and characterized as either a ground- or transition-state structure by frequency calculations. In addition, a qualitative interpretation of the changes in structure and bonding during the course of the reaction is provided. Calculated energy differences cannot, however, be directly compared with experimental values due to the neglect of solvation in the calculations. To remedy this shortcoming, molecular dynamics simulations[20,21] have been performed to account for the effects of solvation by chloroform.[22] The free energy contributions to the conversion of the EDA complex to the transition state and of the transition state to the adduct in chloroform are evaluated using thermodynamic integration techniques.[20,23−26] These corrections are then combined with the energy differences from the density functional calculations to allow a more realistic comparison with experiment.

Hybrid HF/DF Study of the Reaction Path: Structures and Reaction Sequence

We begin by describing the calculated structures of the two reactant molecules, anthracene and TCNE, and of their ionized forms, anthracene$^{•+}$ and TCNE$^{•-}$. This allows for an assessment of the ability of the B3LYP/6-31G(d) method and basis set to reproduce experimental structures for these two well-characterized molecules. An initial review of the structure and bonding found in these species also makes the ensuing discussions of how they change as the reaction proceeds more comprehensible. Finally, knowledge of the properties of TCNE$^{•-}$ and anthracene$^{•+}$ becomes important in later discussions because they represent the limiting case of full electron transfer from anthracene to TCNE and because of the importance of electron donor−acceptor interactions in this reaction.

Table 1 reports the calculated and experimental values of the pertinent bond lengths and angles for the neutral and ionic forms of TCNE and anthracene using the atom numbering system shown in Figure 2 and both the 6-31G(d) and 6-31+G(d,p) basis sets. As the geometries resulting from these two calculations differ negligibly, the discussion will focus specifically on the 6-31G(d) results. While not initially constrained, both TCNE and anthracene are found to be planar and to exhibit D_{2h} symmetry.

In general, excellent agreement is found between the calculated and experimentally determined results. For TCNE, comparison of the calculated structure with the gas-phase electron diffraction[27] structure reveals an average difference of only 0.005

TABLE 1: Comparison of the B3LYP/6-31G(d) and 6-31+G(d,p) Calculated and Experimental Structures of the Neutral and Ionized Forms of Anthracene and TCNE[a]

	anthracene		anthracene$^{•+}$	
parameter	calculated	experiment[b]	calculated	experiment[c]
bond length (Å)				
$C_{11}-C_9$	1.400/1.402	1.392(6)	1.410/1.411	
$C_{11}-C_{12}$	1.445/1.446	1.437(4)	1.441/1.442	
$C_{11}-C_1$	1.430/1.432	1.437(4)	1.414/1.416	
C_1-C_2	1.370/1.372	1.397(4)	1.391/1.392	
C_2-C_3	1.426/1.428	1.422(8)	1.406/1.407	
C_9-H_9	1.088/1.088		1.087/1.087	
C_1-H_1	1.087/1.087	1.085[d]	1.086/1.086	
C_2-H_2	1.087/1.086		1.085/1.085	
average error	0.012/0.012		(n/a)	
bond angle (deg)				
$C_{11}-C_9-C_{14}$	121.8/121.8	122.2(1)	121.9/121.8	
$C_{11}-C_1-C_2$	121.0/121.0	121.1	120.5/120.5	
$C_1-C_{11}-C_{12}$	118.6/118.6	118.8(6)	119.1/119.1	
$C_1-C_2-C_3$	120.4/120.4	120.1	120.4/120.4	
$C_{11}-C_9-H_9$	119.1/119.1		119.1/119.1	
$C_{11}-C_1-H_1$	118.4/118.5		119.3/119.4	
$C_1-C_2-H_2$	120.2/120.2		119.8/119.8	

	TCNE		TCNE$^{•-}$	
parameter	calculated	experiment[e]	calculated	experiment[f]
bond length (Å)				
$C_{25}-C_{26}$	1.372/1.373	1.357(10)	1.442/1.443	1.429(8)
$C_{25}-C_{27}$	1.429/1.430	1.435(10)	1.413/1.413	1.406(9)
$C_{27}-N_{31}$	1.163/1.163	1.162(2)	1.171/1.172	1.170(7)
average error	0.005/0.005		0.005	
bond angle (deg)				
$C_{25}-C_{26}-C_{27}$	121.5/121.5	121.1	121.6/121.7	118.6(6)
$C_{25}-C_{27}-N_{31}$	178.9/178.9	180.0[d]	179.0/179.0	179.0(7)

[a] All species have D_{2h} symmetry. One value is given for each set of symmetry equivalent parameters. Values listed as 6-31G(d)/6-31+G(d,p). [b] Gas-phase electron diffraction study.[28] [c] No experimental structure available. [d] These parameters fixed in structure refinement.[29] [e] Gas-phase electron diffraction study.[27] [f] Solid-state neutron diffraction study.[28]

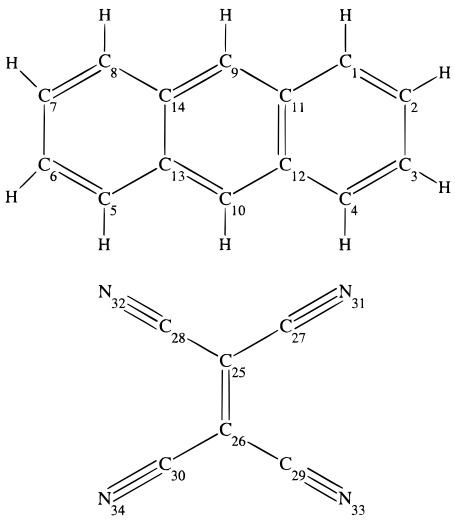

Figure 2. Atom numbering scheme for anthracene and tetracyanoethylene.

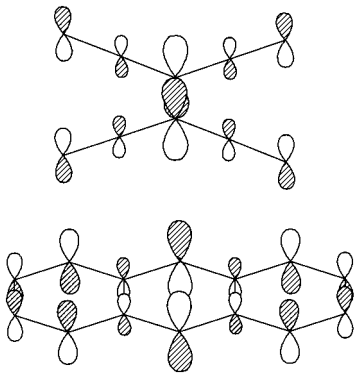

Figure 3. Qualitative molecular orbital diagrams (from UHF/6-31G-(d) calculations) of the LUMO of tetracyanoethylene and the HOMO of anthracene.

Å over all bond lengths. The only significant difference is found in the central C═C bond, which is overestimated by 0.015 Å. A case may be made, however, supporting the accuracy of the calculated result (1.372 Å) based on the significant uncertainty (0.010 Å) in the electron diffraction study and on the results of a recent neutron diffraction study which reports a length of 1.370 Å.[30] Quantitative agreement with experiment is also found for $TCNE^{\bullet-}$. As in the case of TCNE, an average difference of 0.005 Å is found between the calculated and experimental neutron diffraction structures.[28] For both molecules, all of the calculated distances are accurate to well within the commonly accepted threshold of 3 standard deviations (3σ) of experimental uncertainty.

The agreement between the calculated and gas-phase electron diffraction structures of anthracene[29] is also good, as indicated by an average difference of 0.012 Å in bond lengths. While these results agree well on average, a significant deviation (0.027 Å) is found in the C_1-C_2 (and symmetry equivalent) bond distances. As in the case of TCNE, some doubt is cast on this particular experimental bond distance on the basis of the excellent agreement of the calculated result with an X-ray diffraction crystal structure ($\Delta = 0.002$ Å).[31] For $anthracene^{\bullet+}$, the lack of an experimental structure prohibits direct evaluation of the reported results.

All of the structural changes that occur upon oxidation of anthracene and reduction of TCNE to their ionized forms are predictable on the basis of the qualitative molecular orbital diagrams shown in Figure 3. Occupation of the LUMO of TCNE by an additional electron leads to an increased antibonding contribution to the central C═C and the terminal C═N bonds, increasing bond distances relative to those of neutral TCNE. The other four C−C bonds show the opposite effect as the bonding increases between the in-phase orbitals that become occupied on reduction.

Analogous arguments can be offered for anthracene, which loses an electron from its HOMO. Bonding is weakened in the two groups of three in-phase orbitals at the top and bottom of the central six-membered ring, resulting in longer C−C bonds. It should be noted that both the calculated and experimental results show significant bond length alternation for neutral anthracene. Oxidation, however, results in increased uniformity in these bond distances, particularly in the outer rings of $anthracene^{\bullet+}$. This observation will become important in later discussion of the reaction path, where electron donation to TCNE results in the equalization of these distances.

Just as the mechanistic role of the anthracene−TCNE EDA complex has remained elusive, so has its molecular structure. Yet comparison of the calculated structures of the components in the anthracene−TCNE complex relative to their isolated geometries (see Table 2) reveals no real surprises in terms of bond distance changes or the overall planarity of the individual components. Summation of the Mulliken atomic charges[32] for the atoms in both fragments reveals a net donation of 0.20 electron from anthracene to TCNE, indicating that the anthracene fragment is partially cationic and TCNE partially anionic in the complex. On the basis of the extent of electron donation from anthracene to TCNE, it is expected that bond distances found in the complex should be intermediate between those found in the isolated components and their respective ionic forms, and that the structures of the components of the intermediate complex should more closely resemble their neutral than their ionic forms. These predictions are in fact borne out by the numbers shown in Table 2. Later, we discuss the geometric and electronic structure of the intermediate complex as it relates to the other points on the reaction path. Here, we note that the counterpoise correction for basis set superposition error (BSSE)[34,35] in the energy difference between reactants and the complex (including relaxation effects) is 2.1 kcal/mol, smaller than the calculated complexation energy. Since the desirability of accounting for BSSE in the transition state and adduct, which contain partial or full covalent bonds, is controversial, tabulated energies do not include BSSE corrections. Other geometries are also possible for the complex between anthracene and TCNE, and an exhaustive search of all possibilities is impractical. We did, however, begin geometry optimizations with three alternative sets of starting geometries: (1) with TCNE centered over one outer ring of anthracene and oriented as in the complex, (2) with TCNE over the central ring and oriented with its C═C bond parallel to the long axis of anthracene, and (3) with TCNE centered over an outer ring, but oriented as in (2). In all cases of complex formation, the geometry reverted to that reported here. We further note that the calculated HOMO−LUMO gap for the complex, 1.72 eV, is within experimental error of the first charge-transfer band measured for the complex in chloroform, 1.73 eV. Consequently, the calculated complex is real and not simply an artifact of BSSE, its geometry appears reasonable on the basis of the Diels−Alder adduct as well as investigations of other alternative orientations, and its electronic structure accurately reflects the (limited) experimental spectroscopic data. Now, we move to a discussion of the Diels−Alder adduct.

The important structural parameters resulting from the geometry optimizations of the anthracene−TCNE adduct, using both the 6-31G(d) and 6-31+g(d,p) basis sets, are presented in Table 2, along with the corresponding values from the experimental X-ray diffraction structure determined by Karle and Fratini.[33] The initial optimization was begun from the averaged coordinates reported in the experimental study, and no symmetry constraints were imposed. The converged geometry is found to exhibit C_{2v} symmetry, and all calculated bond distances and angles are within experimental uncertainty (where reported). Perhaps the most interesting structural features of this molecule are the long C−C bonds (1.607 Å) formed between the two components of the adduct and the particularly long central C−C bond (1.630 Å) of the TCNE fragment. Both of these bond distances are significantly longer than the "normal" C−C single bond length found in ethane (1.54 Å).

Another notable aspect of the geometries of the adduct is the degree of deviation from planarity found in both the anthracene and TCNE fragments. One way of quantifying this deformation is to sum the angles around C_9/C_{10} in the anthracene fragment and around C_{25}/C_{26} in the TCNE fragment. In the

TABLE 2: Comparison of the B3LYP/6-31G(d) and 6-31+G(d,p) Calculated Bond Distances for Each Stationary Point along the Reaction Coordinate[a]

				adduct	
parameter	reactants	EDA complex	transition state	calculated	experiment[b]
bond length					
$C_{11}-C_9$	1.400/1.402	1.404/1.405	1.446/1.447	1.514/1.515	1.52(0.023)
$C_{11}-C_{12}$	1.445/1.446	1.444/1.445	1.419/1.419	1.402/1.403	1.39(0.031)
$C_{11}-C_1$	1.430/1.432	1.426/1.428	1.406/1.407	1.391/1.392	1.40(0.025)
C_1-C_2	1.370/1.372	1.373/1.375	1.388/1.389	1.398/1.400	1.41(0.027)
C_2-C_3	1.426/1.428	1.421/1.423	1.406/1.407	1.396/1.397	1.40(0.017)
$C_{25}-C_{26}$	1.372/1.373	1.383/1.383	1.482/1.485	1.630/1.632	1.62(0.003)
$C_{25}-C_{27}$	1.429/1.430	1.427/1.428	1.439/1.440	1.472/1.473	1.46(0.017)
$C_{27}-N_{31}$	1.163/1.163	1.164/1.164	1.163/1.163	1.160/1.160	1.15(0.003)
C_9-C_{25}	∞	3.409/3.464	2.166/2.166	1.607/1.608	1.59(0.003)
Σ(angles)					
C_9/C_{10}	360.0/360.0	360.0/360.0	353.4/353.3	335.5/335.2	
C_{25}/C_{26}	360.0/360.0	359.9/359.9	348.8/348.4	331.4/331.3	

[a] Values listed as -31G(d)/6-31+G(d,p). [b] Single-crystal X-ray crystal study. Uncertainties reported to one digit higher accuracy than the value for the parameter; see the original paper for details.[33]

isolated, planar molecules, this sum is 360°. For a tetrahedrally coordinated carbon, the sum is 328.4°. Upon adduct formation and the attendant pyramidalization of these carbon centers, the sum of the angles decreases to 335.5° in the anthracene fragment and 331.4° in the TCNE fragment. These carbon centers are thus identifiable as nearly tetrahedrally coordinated. The calculated CCN angles in the TCNE fragment are bent slightly more in the adduct than in isolated TCNE (176.6° in the adduct vs 178.9° in TCNE). The two outer rings of the anthracene fragment remain essentially planar (0.7° deviation in dihedral angle) and the C−C bond distances become nearly equivalent (ranging from 1.391 to 1.402 Å), indicating an increased benzenoid character relative to the bond distances in isolated anthracene.

The transition-state geometry resulting from our calculations is reported in Table 2. In most studies of Diels−Alder reactions, the question arises whether the correct transition state lies on a synchronous or asynchronous path between reactants and product (i.e., are the new bonds formed simultaneously and with equal length or not?).[36,37] The synchronous nature of the anthracene−TCNE Diels−Alder reaction was confirmed by attempting to locate asynchronous transition states by starting with six lower symmetry initial structures. Symmetry around the C_2 rotation axis and about one of the two mirror planes was broken in four of these initial structures, which were generated by holding the anthracene fragment stationary while translating (two structures) and rotating (two structures) the TCNE fragment. The fifth structure, generated by rotation about the C_2 axis, had no planes of symmetry, but retained its C_2 rotational symmetry. Finally, a nonsymmetric (C_1) structure was generated by a combination of translation and rotation. All successful calculations converged to structures very similar to the C_{2v} geometry reported here. These results lead to the conclusion that the symmetric transition state is the only one of significance in this reaction. Once the converged transition-state structure was found, a frequency calculation was performed to confirm that the transition state has one imaginary frequency. Next, we used the intrinsic reaction coordinate (IRC) method[18,19] to confirm that the EDA complex is the minimum energy structure on the reactant side of the transition state, and that the adduct is on the product side for the anthracene/TCNE reaction.

One of the few experimentally accessible indicators of the symmetry of the transition structure and its position along the reaction coordinate is the secondary kinetic isotope effect (k_H/k_D).[38] As part of their early studies, Brown and co-workers reported a secondary kinetic isotope effect (SKIE) of $k_H/k_D = 1.17 \pm 0.05$ for the dissociation reaction of the anthracene−TCNE adduct.[39] To check the accuracy of the present calculations, the SKIE has been calculated for the retro-Diels−Alder cycloaddition (dissociation of the adduct) for this system. While more advanced ways of calculating isotope effects exist,[40−42] k_H/k_D may be estimated by simply employing the Arrhenius equation and estimates of activation energies. Estimated activation energies at 323 K were calculated by using the zero point corrected energies of the adduct and transition state. Additionally, it was assumed that the preexponential factors for the unsubstituted reaction and the deuterium-substituted (at C_9 and C_{10} of anthracene) reactions are equivalent, and therefore cancel when taking the ratio k_H/k_D. Despite the use of this approximate method, a SKIE of 1.21 is calculated, within experimental error of the measured value of 1.17 ± 0.05.[39]

As a more direct means of evaluating the position of the calculated transition-state structure along the reaction path, its structure is compared to those of the reactants and products in Table 2. The transition-state structure is more adduct-like than complex-like, on the basis of the similarity of bond lengths and angles, as well as in terms of interfragment separation. For example, the distance between the midpoints of the C_9-C_{10} axis of anthracene and the $C_{25}-C_{26}$ bond of TCNE was calculated. In the EDA complex, transition state, and adduct these distances are 3.33, 2.08, and 1.53 Å, respectively. The differences between these distances show that the interfragment separation in the transition state is 1.25 Å shorter than that in the complex and only 0.55 Å longer than that in the adduct, indicating a late transition structure. In addition the dipole moment of the transition state, 8.1 D, is closer to that of the adduct, 8.0 D, than that of the EDA complex, 3.4 D. The large difference between the complex and transition-state dipole moments (4.7 D) reflects the increase in the extent of charge transfer from 0.20 to 0.46 electron. The very small difference in dipole moment between the transition state and adduct (0.1 D) is accompanied by a correspondingly smaller change in the extent of electron donation, from 0.46 to 0.32 electron. These results confirm the idea that the transition state is more structurally and electronically similar to the adduct than to the EDA complex.

Energetics of the Reaction in the Gas Phase and in Chloroform

Having located and structurally characterized all species along the calculated minimum energy reaction path, their relative

TABLE 3: B3LYP Calculated Electronic and Gibbs Free Energy Differences for the Anthracene/TCNE Reaction (kcal/mol, 298.15 K, Chloroform Solvent)

	6-31G(d)	6-31+G(d,p)	experiment[b]
	$\Delta E_{(elec+zpe)}$[a]		
reactants → complex ($\Delta E°_{comp}$)	−5.22	−3.76	
reactants → transition state ($\Delta E^{‡}_{expt}$)	18.90	20.36	
complex → transition state ($\Delta E^{‡}$)	24.12	24.13	
adduct → transition state ($\Delta E^{‡}_{retro}$)	19.41	19.00	
complex → adduct ($\Delta E°$)	4.71	5.13	
reactants → adduct ($\Delta E°_{expt}$)	−0.51	1.37	
	$\Delta E_{(elec+zpe)} + \Delta\Delta G_{(solv)}$[c]		
reactants → complex ($\Delta G°_{comp}$)			−3.5
reactants → transition state ($\Delta G^{‡}_{expt}$)			16.5
complex → transition state ($\Delta G^{‡}$)	20.08	20.09	20.0
adduct → transition state ($\Delta G^{‡}_{retro}$)	19.98	19.57	24.6
complex → adduct ($\Delta G°$)	1.24	1.66	−4.6
reactants → adduct ($\Delta G°_{expt}$)			−8.1

[a] All electronic energies corrected for zero-point vibrational energy at the B3LYP/6-31G(d) level. [b] Reference 43. [c] Estimated value based on correlation with a series of 9-substituted anthracene/chloranil complexes. See Reference 2.

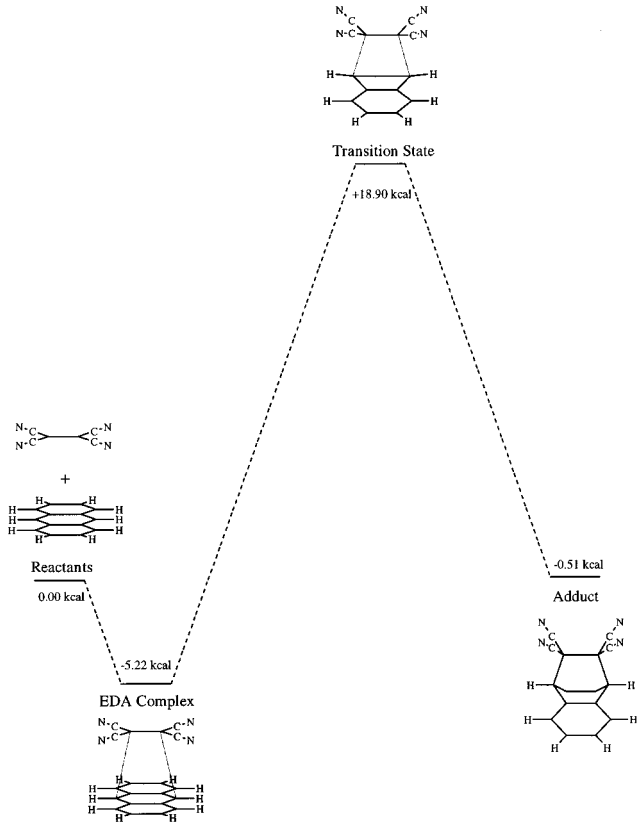

Figure 4. Qualitative reaction path diagram illustrating structures and B3LYP/ 6-31G(d) calculated energies, relative to the reactants.

energies may now be evaluated and compared with experimental determinations. The B3LYP/6-31G(d) energies, corrected for zero-point vibrational effects, are used as the baseline in this section, and the energies from the B3LYP/6-31+G(d,p) calculations are compared to determine the effect of including diffuse functions and extra polarization functions on hydrogen in the basis set. All energy differences discussed in this section are summarized in Table 3, and an approximate energy level diagram is given in Figure 4. All calculated energies are also provided as Supporting Information. Quantitative agreement between these calculated energy changes and experimental results is not to be expected because the calculations correspond to a hypothetical experimental arrangement at 0 K in which the reacting species are completely isolated from any external perturbations. Obviously, these conditions are not met in a study conducted in chloroform solution at room temperature.

It is necessary, therefore, to consider explicit solvent−solute interactions. This was accomplished by molecular dynamics (MD) simulations of the reaction path in a bath of chloroform molecules. In molecular dynamics simulations, the interactions between solute and solvent are treated classically using parameters (geometries, charges, and force constants) determined from the quantum chemical calculations.[20−22]

Calculated Gibbs free energies are reported for the conversion of the EDA complex to the transition structure and its further conversion to the adduct. Molecular dynamics simulations were not performed for the conversion of reactants to the EDA complex because the free energy differences are expected to be less than the error limits of the calculation, on the basis of experimental studies in a series of chloromethanes.[43] Details of how these simulations were performed may be found in the Appendix.

Before proceeding, we note that it is not strictly correct to compare the summed zero-point electronic energies and free energy differences obtained from the molecular dynamics simulations with experimental thermodynamic parameters, due to the neglect of enthalpic and entropic contributions to the internal free energy of the solute species at room temperature. Currently, the only tractable method of evaluating these thermal corrections is the use of the rigid rotor, harmonic oscillator approximation for an ideal gas.[44,45] In many situations, these approximations are satisfactory for the evaluation of reaction thermodynamics, but the current situation is more complicated. Both the EDA complex and the transition-state species have a number of very low frequency, interfragment normal modes that are not well represented as harmonic vibrations. Treatment of these interfragment stretches, rotations, and translations as harmonic oscillations introduces significant error into the thermal corrections. An additional complication results from the excitation of low-frequency modes by the thermal energy, *RT*, which is 231 cm^{-1} at 298.15 K. Both the EDA complex and the transition state have 13 frequencies below 231 cm^{-1}, including those mentioned above. Rather than introduce unpredictable errors by applying inappropriate approximations, the choice was made to simply use the zero-point electronic energies in conjunction with the molecular dynamics derived solvation corrections to approximate the total free energy changes in this reaction. Ongoing work in developing integrated quantum mechanics/molecular dynamics methods may allow more satisfactory treatment of these issues in the future.

The first step in this reaction is the barrierless, exothermic formation of the EDA complex from the separated reactants. At the B3LYP/6-31G(d) level the energy change for complex formation ($\Delta E°_{comp}$) is −5.22 kcal/mol, and the 6-31G+(d,p) calculation predicts a change of −3.76 kcal/mol. Unfortunately, no direct experimental measurements of the EDA complex's thermodynamic stability have been made.

The next step along the reaction coordinate is the activation of the EDA complex to the transition structure. For this process the 6-31G(d) and 6-31+G(d,p) calculations differ by only 0.01 kcal/mol, with values of 24.12 and 24.13 kcal/mol, respectively. The molecular dynamics simulations of this reaction step predict a decrease in activation barrier of −4.04 kcal/mol when the reaction is carried out in a chloroform solution vs the gas phase. Adding this correction to the calculated energy differences gives values of 20.08 and 20.09 kcal/mol for the two basis sets used. The experimentally observed activation free energy ($\Delta G^{‡}_{expt}$)

is actually the sum of the $\Delta G°_{comp}$ and the free energy change associated with conversion of the complex to the transition-state structure ($\Delta G^{‡}$), i.e., the free energy change of conversion of the reactants to the transition state. When the $\Delta G°_{comp}$ contribution is removed from the total $\Delta G^{‡}_{expt}$, a value suitable for comparison with the calculated $\Delta G^{‡}$ is obtained. The experimentally derived value is found to be 20.0 kcal/mol,[43] which is in quantitative agreement with the molecular dynamics corrected calculated values.

The final step in the reaction is the conversion of the transition-state structure to the adduct. This discussion will focus on the opposite process, the conversion of the adduct to the transition state, to comport with the experimentally measured activation free energy for the retro-cycloaddition reaction, $\Delta G^{‡}_{retro}$. Again close agreement is found between the 6-31G(d) and 6-31+G(d,p) calculations with values of 19.41 and 19.01 kcal/mol, respectively. The molecular dynamics simulations reveal an increase of 0.57 kcal/mol in this barrier in chloroform relative to the gas phase. This correction yields values of 19.98 and 19.57 kcal/mol, respectively. The experimentally determined retro-activation energy is 24.6 kcal/mol,[46] indicating an error in the calculated values of 4.6−5 kcal/mol. On the basis of the excellent agreement between calculation and experiment for the forward activation free energy, it would appear that the energy of the adduct relative to the transition state is overestimated by the B3LYP method. This explanation was tested by performing MP2/6-31G(d) single-point calculations on the B3LYP/6-31G(d) optimized structures of the transition state and adduct. When combined with the B3LYP/6-31G(d) zero-point corrections and the molecular dynamics solvation correction, the calculated retro-activation energy and free energy are 24.42 and 24.99 kcal/mol, respectively. This MP2-derived free energy change for the retro-cycloaddition reaction agrees quantitatively, in this case, with the experimental value of 24.6 kcal/mol (other MP2/6-31G(d) energies are reported in the Supporting Information).

Donor−Acceptor Assistance in Stabilizing the Reaction Path

The first step along the anthracene/TCNE reaction path is the formation of the intermediate EDA complex between anthracene and TCNE. The relative orientation of the two addends in the complex is easily predictable, in a qualitative sense, by matching the symmetries and maximizing the overlap of frontier molecular orbitals. It is apparent from Figure 3 that alignment of the π HOMO of anthracene, having its maximal AO coefficients of opposite signs on C_9 and C_{10}, with the π^* LUMO of TCNE, having its corresponding largest and opposite signed AOs on C_{25} and C_{26}, provides an ideal orientation for electron donation from the electron-rich HOMO of anthracene to the energetically low-lying LUMO of TCNE. Using the qualitatively correct Mulliken atomic charges from the B3LYP/6-31G(d) calculations, a net donation of 0.20 electron from anthracene to TCNE is found at this point on the reaction path. As previously detailed, all changes in bond distances between the isolated addends and the intermediate complex are consistent with this electron donation, as these properties become more similar to those found in their corresponding ionic forms.

Further examination of the structure calculated for the transition state reveals considerable changes in the geometries of the addends, most dramatically illustrated by their deformation from planarity. One way to explain these observations is to note that the partially charged addends should be less resistant to deformation than are their neutral analogues. To test this idea, single-point calculations were done to compare the relative

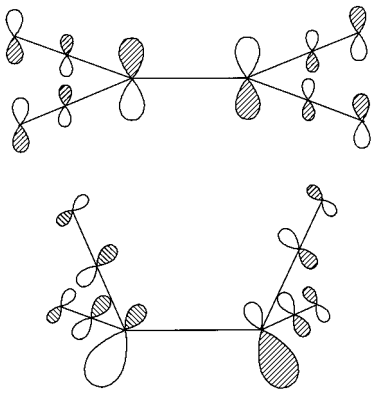

Figure 5. Qualitative molecular orbital diagram (from UHF/6-31G(d) calculations) illustrating the hybridization of the LUMO of the tetracyanoethylene fragment upon conversion from EDA complex to transition state.

energies of the neutral and ionic forms of the addends in both their planar and deformed (at the geometry found in the transition state) structures. For neutral anthracene, the difference in energy between the planar and pyramidal structures is 26.8 kcal/mol while it is 23.2 kcal/mol for the cationic form, meaning that it requires 3.6 kcal/mol less to deform the cation to the transition structure than the neutral. Similarly, for neutral TCNE an energy difference of 23.7 kcal/mol is found between the planar and pyramidal geometries, much more than the 12.8 kcal/mol difference found for the anionic form, resulting in an energy savings of 10.9 kcal/mol. Of course, these numbers cannot be interpreted quantitatively because a full electron has been added or removed rather than the partial electron donation that actually occurs. So while the result is exaggerated, the qualitative prediction that deforming the addends from their initial planar structure to the pyramidal form of the transition state is energetically less costly after electron donation is still valid.

The origin of the stabilization of the ionic forms relative to the neutral forms in the pyramidal geometries becomes apparent upon closer inspection of the structural and underlying orbital changes that take place during the conversion. As previously mentioned, removal of electron density from the HOMO of anthracene weakens the bonding interactions that enforce planarity on the central ring of the molecule, the two groups of in-phase p_z orbitals at the top ($C_{14}-C_9-C_{11}$) and bottom ($C_{13}-C_{10}-C_{12}$) of the ring (see the orbital diagram of Figure 3 and the atom numbering in Figure 1). Reducing the π bonding in these two allylic moieties clearly makes them less resistant to an out of plane deformation. Removing electron density from the HOMO also reduces the tendency toward bond localization on the two peripheral rings, providing the additional stabilization inherent in the more benzenoid structure of these rings. This change is clearly reflected in their geometries, which are somewhat localized in the isolated molecule and intermediate but much more similar to that of benzene in the transition state. In view of these arguments, the energy differences predicted above are qualitatively reasonable.

In the case of TCNE, the reasons for stabilization of the transition structure in the anion relative to the neutral are not as immediately apparent. At first glance (see Figure 3), addition of an electron to the LUMO of TCNE would seem to hinder rather than aid the stabilization of the deformed geometry, due to the increased population of the two sets of three bonding AOs located on C_{27}, C_{25}, C_{28} and C_{30}, C_{26}, C_{29}. Reinforcement of the bonding in these two fragments would appear to retard the process of pyramidalization. As shown in Figure 5, however, little bonding overlap is lost in these C−C bonds upon

conversion to a pyramidal geometry due to mixing of the p_x and p_z AOs of C_{25} and C_{26} in a direction conducive to bonding to the p AOs on the carbons of the cyano groups in their new geometrical orientation. In fact, this hybridization also reduces the antibonding interaction between C_{25} and C_{26} as the larger lobes of the hybrid p orbitals are rotated away from one another during the pyramidalization. This latter stabilization is further increased by the dramatic (0.110 Å) lengthening of the $C_{25}-C_{26}$ bond distance that takes place during the formation of the transition state.

Conclusions

This work provides the first computational confirmation of the participation of an electron donor−acceptor (EDA) complex as an intermediate in the Diels−Alder cycloaddition reaction between anthracene and TCNE. Prior to this work, only indirect experimental evidence was available to support this postulate, for the related but distinct reaction of 9,10-dimethylanthracene with TCNE.[9] This work also provides a physical interpretation of how the initial formation of the EDA complex stabilizes the bimolecular system prior to, and assists in, its activation to the transition state.

The geometry of the intermediate complex is predictable using frontier molecular orbital ideas of how the HOMO of an electron donor (anthracene) should be oriented to maximize the overlap with the LUMO of the corresponding electron acceptor (TCNE). This arrangement, in conjunction with the high electron affinity of TCNE and the low ionization potential of anthracene, naturally results in the donation of electron density from donor to acceptor, creating a stabilized EDA complex. As the reaction proceeds from the intermediate complex to the transition state, the extent of electron donation from anthracene to TCNE also continues to increase and reaches a maximum of 0.46 electron at the transition-state structure. The synergistic processes of electron donation and geometrical distortion reinforce one another, providing the driving force for the conversion from the intermediate to transition state. The subsequent, final phase of the reaction is characterized by relatively large geometrical changes in the core of the evolving adduct where the new bonds are being formed between the anthracene and TCNE fragments. The electronic redistribution attendant upon the formation of the two new covalent bonds is reflected in the charge separation, which reaches a maximum of 0.46 electron in the transition state and decreases to 0.32 electron in the adduct. Thus, electron donor−acceptor interactions, from initiation of this reaction to its completion, are significant factors.

This work also illustrates the aptitude of density functional theory, specifically the B3LYP method, to predict qualitatively correct relative energies of the various stationary structures along the reaction path. Overall, the B3LYP method delivers mixed results for this system. It performs quite well for the relative energetics of the reactants, the complex, and the transition state. Evaluating the relative energy of the adduct, which is overestimated with respect to all other species on the reaction path, appears problematical. This error does not appear to originate from basis set problems as the calculated energy differences vary by less than 0.5 kcal/mol for both the forward and reverse activation processes. The 6-31G(d) basis set also predicts the reactants to be about 1.5 kcal/mol less stable than the 6-31+G(d,p) basis set, as manifested in the more exothermic values calculated for both complex formation and the overall energy of reaction. The range of basis sets employed in this study is, however, limited, and future work using larger sets might yield improved results.

Inclusion of molecular dynamics corrections to account for solvent effects on reaction energetics is found to be very important in this reaction. In every case, the correction brings the B3LYP calculated energies into closer agreement with experiment. The most notable success is the outstanding agreement in the forward activation energy, $\Delta G^{\ddagger}$, which is in error by less that 0.1 kcal/mol after correction for solvation by chloroform. The correction also improves the retro-activation energy and the energy difference between the EDA complex and adduct, but in both cases qualitative differences remain due to the large error in the B3LYP calculated energies. While performing the molecular dynamics simulations to determine these corrections is not a trivial process, the improvements in accuracy that may be realized are significant.

Acknowledgment. We are grateful to the National Science Foundation/Metacenter Allocations Committee and its successor, the NSF/National Resource Allocations Committee, for providing supercomputer time at the National Center for Supercomputing Applications. We also thank the NSF, IBM Corp., and Silicon Graphics Inc. for providing support for supercomputers located at the University of Oklahoma. K.E.W. thanks A. Kurt Grafton and Kevin S. Raymond for helpful discussions during the course of this work.

Appendix: Details of the Molecular Dynamics Simulations

For the purpose of comparison with experiment, it was necessary to evaluate the solvation contribution to the total free energy change for three segments of the reaction of anthracene and TCNE: EDA complex to transition state, transition state to adduct, and EDA complex to adduct.

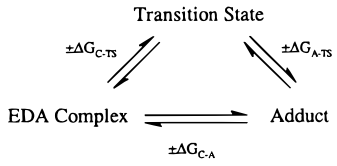

The $\pm\Delta G$ labels in the diagram indicate that the perturbations were carried out in both the forward and reverse directions. The values of ΔG were calculated using thermodynamic integration[20,23−26] according to the following equation:

$$\Delta G = \int_0^1 \frac{\partial G(\lambda)}{\partial \lambda}\, d\lambda = \int_0^1 \left\langle \frac{\partial H(\lambda)}{\partial \lambda} \right\rangle_\lambda d\lambda$$

This method represents the system by a Hamiltonian, $H(\lambda)$, where the parameter λ is incremented from 0, corresponding to the initial state, to 1, corresponding to the final state. For example, in converting from the EDA complex to the adduct, one would define $H(0) = H_{(\text{EDA complex})}$ and $H(1) = H_{(\text{adduct})}$, and vary λ in regular increments from 0 to 1:

$$H = \lambda H_1 + (1 - \lambda) H_0$$

This procedure slowly converts the Hamiltonian of the EDA complex to that of the adduct and integrates the small energy changes at each step over the entire perturbation path. The result is a total free energy difference between the EDA complex and the adduct. All molecular dynamics simulations were performed with the AMBER5.0 package.[23]

To assess the convergence of the calculated free energy differences, each of the six gas-phase and six solution-phase perturbations were performed at two time lengths: 52.5 and

TABLE 4: Simulation Details for the Reaction of Anthracene and TCNE in the Gas Phase and Chloroform Solution (All Energies in kcal/mol)[a]

	52.5 ps[c]	105 ps[c]	315 ps[b,c]
ΔG_{vap}			
complex → TS	−25.82(0.01)	−25.61(0.10)	−25.68(0.05)
TS → adduct	+11.10(0.21)	+11.00(0.19)	+10.96(0.09)
complex → adduct	−15.10(0.09)	−14.76(0.20)	n/a
ΔG_{soln}			
complex → TS	−29.15(0.36)	−29.64(0.21)	−29.72(0.24)
TS → adduct	+11.40(0.41)	+11.34(0.57)	+11.53(0.03)
complex → adduct	−18.09(0.03)	−18.27(0.58)	n/a
$\Delta\Delta G$			
complex → TS	−3.31	−3.92	−4.04
TS → adduct	+0.30	+0.34	+0.57
complex → adduct	−2.99	−3.51	n/a
no. of steps (λ)	21	21	21
no. of equilibration steps/λ	1000	2000	6000
no. of data collection steps/λ	1500	3000	9000

[a] Numbers in parentheses are the difference in free energy changes (hysteresis) for the forward and reverse simulations of each process. [b] 315 ps runs not performed for the complex → adduct process. [c] Length of simulation.

105 ps. The conversions of the EDA complex to the transition state and the transition state to the adduct, both in the gas phase and in chloroform, were also performed over a 315 ps interval. In each case, the initial structures were equilibrated for 200 ps prior to the simulation being started. For each time length, the runs were composed of 21 windows, so $d\lambda = 0.05$ for each simulation. The increases in total time are due to the use of more steps of equilibration and data collection for each value of λ, as reported in the bottom block of Table 4.

Since the gas-phase energy differences for each of these processes had already been calculated quantum mechanically, only the free energy changes due to solvation ($\Delta\Delta G$ values) were of interest. These were obtained by carrying out the six simulations, illustrated above, first in the absence of solvent and again in a box of chloroform solvent molecules. $\Delta\Delta G$ is obtained by taking the difference in the gas- and solution-phase free energy differences:

$$\Delta\Delta G = \Delta G_{soln} - \Delta G_{vap}$$

The final values for ΔG_{soln}, ΔG_{vap}, and $\Delta\Delta G$ are listed in Table 4.

Each box contained 1 solute molecule and 386 chloroform molecules. The dimensions of the boxes were approximately 38 Å on a side, but since the simulations were done under the condition of constant pressure, rather than constant volume, the dimensions varied somewhat during the runs. The size of the box was dictated by the need to use a relatively long nonbonded cutoff of 15 Å. (Although cutting off long-range interactions introduces some error in calculated energy differences, continuum dielectric models may be used to estimate the error.[47] Using eq 19 of ref 47 implies that the error in the calculated activation energy due to differences in dipole moments, approximately 0.08 kcal/mol, is tiny.) When the solvent boxes are created around the solute molecule, the solvent molecules are placed in a regular array. It was necessary, therefore, to equilibrate each box for approximately 200 ps before the perturbation runs were begun to allow the solvent molecules to relax into a more reasonable configuration around the solute. For each equilibration run a graph of energy vs time was constructed. In each case the energy was found to plateau, indicating equilibration, before 200 ps had elapsed. All runs were done using the SHAKE algorithm[48,49] to maintain constant bond lengths and a time step of 1 fs. Since perturbations were performed in both directions, the single wide sampling procedure was used.

Force field parameters recently developed and reported by Kollman and co-workers were used for the chloroform molecules.[50] Atomic charges and force constants for the solutes were derived from the B3LYP/6-31G(d) calculations. Harmonic force constants in internal coordinates were recalculated using GAMESS[51] from the Cartesian force constants produced by GAUSSIAN94.[17] The internal coordinate definitions were made according to the suggestions of Boatz and Gordon.[52] The charges were calculated using the ChelpG charge-fitting algorithm.[53,54] All other parameters were selected by analogy from the AMBER force field.[55] The Supporting Information includes the B3LYP/6-31G(d) calculated Cartesian coordinates for the EDA complex, transition state, and adduct as well as the force field parameters used in the molecular dynamics simulations.

Supporting Information Available: Tables of optimized structures for the anthracene−TCNE electron donor−acceptor complex, transition state, and Diels−Alder adduct, force field parameters for anthracene and TCNE, and quantum chemically derived energies. This material is available free of charge via the Internet at http://pubs.acs.org.

References and Notes

(1) Diels, O.; Alder, K. *Justus Liebigs Ann. Chem.* **1928**, *460*, 98−122.
(2) Lotfi, M.; Roberts, R. M. G. *Tetrahedron* **1979**, *35*, 2123-2129.
(3) Fukuzumi, S.; Kochi, J. K. *Tetrahedron* **1982**, *38*, 1035−1049.
(4) Hilinski, E. F.; Masnovi, J. M.; Amatore, C.; Kochi, J. K.; Rentzepis, P. M. *J. Am. Chem. Soc.* **1983**, *105*, 6167−6168.
(5) Hilinski, E. F.; Masnovi, J. M.; Kochi, J. K.; Rentzepis, P. M. *J. Am. Chem. Soc.* **1984**, *106*, 8071−8077.
(6) Masnovi, J. M.; Seddon, E. A.; Kochi, J. K. *Can. J. Chem.* **1984**, *62*, 2552−2559.
(7) Masnovi, J. M.; Kochi, J. K.; Hilinski, E. F.; Rentzepis, P. M. *J. Phys. Chem.* **1985**, *89*, 5387−5395.
(8) Epiotis, N. D. *J. Am. Chem. Soc.* **1972**, *94*, 1924−1934.
(9) Kiselev, V. D.; Miller, J. G. *J. Am. Chem. Soc.* **1975**, *97*, 4036−4039.
(10) Sustmann, R.; Dern, M.; Kasten, R.; Sicking, W. *Chem. Ber.* **1987**, *120*, 1315−1322.
(11) Kim, E.; Christi, M.; Kochi, J. K. *Chem. Ber.* **1990**, *123*, 1209−1218.
(12) Sustmann, R.; Korth, H.-G.; Nuchter, U.; Siangouri-Feulner, I.; Sicking, W. *Chem. Ber.* **1991**, *124*, 2811−2817.
(13) Houk, K. N.; Rondan, N. G.; Mareda, J. *Tetrahedron* **1985**, *41*, 1555−1563.
(14) Parr, R. G.; Yang, W. *Annu. Rev. Phys. Chem.* **1995**, *46*, 701−728.
(15) Kohn, W.; Becke, A. D.; Parr, R. G. *J. Phys. Chem.* **1996**, *100*, 12974−12980.
(16) Baerends, E. J.; Gritsenko, O. V. *J. Phys. Chem. A* **1997**, *101*, 5383−5403.
(17) Frisch, M. J.; Trucks, G. W.; Schlegel, H. B.; Gill, P. M. W.; Johnson, B. G.; Robb, M. A.; Cheeseman, J. R.; Keith, T. A.; Petersson, G. A.; Montgomery, J. A.; Raghavachari, K.; Al-Laham, M. A.; Zakrzewski, V. G.; Ortiz, J. V.; Foresman, J. B.; Peng, C. Y.; Ayala, P. A.; Wong, M. W.; Andres, J. L.; Replogle, E. S.; Gomperts, R.; Martin, R. L.; Fox, D. J.; Binkley, J. S.; Defrees, D. J.; Baker, J.; Stewart, J. P.; Head-Gordon, M.; Gonzalez, C.; Pople, J. A. *GAUSSIAN94 (Revisions B2, B3, D1, and D2)*; Gaussian, Inc.: Pittsburgh, 1995.
(18) Gonzalez, C.; Schlegel, H. B. *J. Chem. Phys.* **1989**, *90*, 2154.
(19) Gonzalez, C.; Schlegel, H. B. *J. Phys. Chem.* **1990**, *94*, 5523.
(20) Kollman, P. *Chem. Rev.* **1993**, *93*, 2395−2417.
(21) van Gunsteren, W. F.; Berendsen, H. K. C. *Angew. Chem.* **1990**, *102*, 1020−1051.
(22) Jorgensen, W. L. *Acc. Chem. Res.* **1989**, *22*, 184−189.
(23) Case, D. A.; Pearlman, D. A.; Caldwell, J. W.; Cheatham, T. E., III; Ross, W. S.; Simmerling, C. L.; Darden, T. A.; Merz, K. M.; Stanton, R. V.; Cheng, A. L.; Vincent, J. J.; Crowley, M.; Ferguson, D. M.; Radmer,

R. J.; Seibel, G. L.; Singh, U. C.; Weiner, P. C.; Kollman, P. A. *AMBER5*; University of California: San Francisco, 1997.
(24) Mezei, M.; Swaminathan, S.; Beveridge, D. L. *J. Am. Chem. Soc.* **1978**, *100*, 3255−3256.
(25) Mezei, M.; Beveridge, D. L. *Ann. N. Y. Acad. Sci.* **1986**, *482*, 1−23.
(26) Van Gunsteren, W. F.; Weiner, P. K. *Computer Simulation of Biomolecular Systems*; Escom: Leiden, 1989.
(27) Hope, H. *Acta Chem. Scand.* **1968**, *22*, 1057−1058.
(28) Zheludev, A.; Grand, A.; Ressouche, E.; Schweizer, J.; Morin, B. G.; Epstein, A. J.; Dixon, D. A.; Miller, J. S. *J. Am. Chem. Soc.* **1994**, *116*, 7243−7249.
(29) Ketkar, S. N.; Kelley, M.; Fink, M.; Ivey, R. C. *J. Mol. Struct.* **1981**, *77*, 127−138.
(30) Druck, U.; Guth, H. *Z. Kristallogr.* **1982**, *161*, 103−110.
(31) Cruickshank, D. W. J.; Sparks, R. A. *Proc. R. Soc. London, Ser. A* **1961**, *258*, 270.
(32) Mulliken, R. S. *J. Chem. Phys.* **1955**, *23*, 1833−1840.
(33) Karle, I. L.; Fratini, A. V. *Acta Crystallogr.* **1970**, *B26*, 596−606.
(34) van Duijneveldt, F. B.; van Duijneveldt-van de Rijdt, J. G. C. M.; van Lenthe, J. H. *Chem. Rev.* **1994**, *94*, 1873.
(35) Boys, S. F.; Bernardi, F. *Mol. Phys.* **1970**, *19*, 553.
(36) Sauer, J.; Sustmann, R. *Angew. Chem., Int. Ed. Engl.* **1980**, *19*, 779−807.
(37) Borden, W. T.; Loncharich, R. J.; Houk, K. N. *Annu. Rev. Phys. Chem.* **1988**, *39*, 213−236.
(38) Taagepera, M.; Thornton, E. R. *J. Am. Chem. Soc.* **1972**, *94*, 1168−1177.
(39) Brown, P.; Cookson, R. C. *Tetrahedron* **1965**, *21*, 1991−1998.
(40) Bigelseisen, J.; Mayer, M. G. *J. Chem. Phys.* **1947**, *15*, 261−267.
(41) Wolfsberg, M. *Acc. Chem. Res.* **1972**, *5*, 225−233.
(42) Saunders: M.; Laidig, K. E.; Wolfsberg, M. *J. Am. Chem. Soc.* **1989**, *111*, 8989−8994.
(43) Lotfi, M.; Roberts, R. M. G. *Tetrahedron* **1979**, *35*, 2137−2141.
(44) Forst, W. *Theory of Unimolecular Reactions*; Academic: New York, 1973.
(45) Laidler, K. J.; Meiser, J. H. *Physical Chemistry*; Benjamin/Cummings: Menlo Park, CA, 1982.
(46) Kiselev, V. D.; Malkov, V. B.; Konovalov, A. I. *Russ. J. Org. Chem.* **1990**, *26*, 191−200.
(47) Beveridge, D. L.; Schnuelle, G. W. *J. Phys. Chem.* **1975**, *79*, 2562−2566.
(48) van Gunsteren, W. F.; Berendsen, H. J. C. *Mol. Phys.* **1977**, *34*, 1311−1327.
(49) van Gunsteren, W. F.; Berendsen, H. J. C. *J. Comput. Phys.* **1977**, *23*, 327−341.
(50) Fox, T.; Thomas, B. E., IV; McCarrick, M.; Kollman, P. A. *J. Phys. Chem.* **1996**, *100*, 10779−10783.
(51) Schmidt, M. W.; Baldridge, K. K.; Boatz, J. A.; Jensen, J. H.; Koseki, S.; Gordon, M. S.; Nguyen, K. A.; Windus, T. L.; Elbert, S. T. *QCPE Bull.* **1990**, *10*, 304.
(52) Boatz, J. A.; Gordon, M. S. *J. Phys. Chem.* **1989**, *93*, 1819−1826.
(53) Breneman, C. M.; Wiberg, K. B. *J. Comput. Chem.* **1990**, *11*.
(54) Chirlian, L. E.; Francl, M. M. *J. Comput. Chem.* **1987**, *8*.
(55) Cornell, W. D.; Cieplak, P.; Bayly, C. I.; Gould, I. R.; Merz, K. M., Jr.; Ferguson, D. M.; Spellmeyer, D. C.; Fox, T.; Caldwell, J. W.; Kollman, P. A. *J. Am. Chem. Soc.* **1995**, *117*, 5179−5197.